ORIGINAL RESEARCH

Cellulose Nanofiber-Coated Perfluoropentane Droplets: Fabrication and Biocompatibility Study

Ksenia Loskutova [ID][1], Mar Torras [ID][1], Ying Zhao [ID][2], Anna J Svagan [ID][3], Dmitry Grishenkov [ID][1]

[1]Department of Biomedical Engineering and Health Systems, KTH Royal Institute of Technology, Huddinge, SE-141 57, Sweden; [2]Department of Laboratory Medicine, Karolinska Institute, Huddinge, SE-141 57, Sweden; [3]Department of Fibre and Polymer Technology, KTH Royal Institute of Technology, Stockholm, SE-100 44, Sweden

Correspondence: Ksenia Loskutova, Department of Biomedical Engineering and Health Systems, KTH Royal Institute of Technology, Hälsovägen 11C, Huddinge, SE-14157, Sweden, Tel +46 707 26 76 77, Email ksenial@kth.se

Purpose: To study the effect of cellulose nanofiber (CNF)-shelled perfluoropentane (PFP) droplets on the cell viability of 4T1 breast cancer cells with or without the addition of non-encapsulated paclitaxel.

Methods: The CNF-shelled PFP droplets were produced by mixing a CNF suspension and PFP using a homogenizer. The volume size distribution and concentration of CNF-shelled PFP droplets were estimated from images taken with an optical microscope and analyzed using Fiji software and an in-house Matlab script. The thermal stability was qualitatively assessed by comparing the size distribution and concentration of CNF-shelled PFP droplets at room temperature (~22°) and 37°C. The cell viability of 4T1 cells was measured using a 3-[4,5-dimethylthiazol-2yl]-2,5-diphenyltetrazolium bromide (MTT) assay. Additionally, a hemolysis assay was performed to assess blood compatibility of CNF-shelled PFP droplets.

Results: The droplet diameter and concentration of CNF-shelled PFP droplets decreased after 48 hours at both room temperature and 37°C. In addition, the decrease in concentration was more significant at 37°C, from $3.50 \pm 0.64 \times 10^6$ droplets/mL to $1.94 \pm 0.10 \times 10^6$ droplets/mL, than at room temperature, from $3.65 \pm 0.29 \times 10^6$ droplets/mL to $2.56 \pm 0.22 \times 10^6$ droplets/mL. The 4T1 cell viability decreased with increased exposure time and concentration of paclitaxel, but it was not affected by the presence of CNF-shelled PFP droplets. No hemolysis was observed at any concentration of CNF-shelled PFP droplets.

Conclusion: CNF-shelled PFP droplets have the potential to be applied as drug carriers in ultrasound-mediated therapy.

Keywords: cell viability, ultrasound-mediated therapy, paclitaxel, cellulose nanofibers, biocompatibility, 4T1, Pickering emulsion

Introduction

Gas-filled microbubbles have been utilized in ultrasound-mediated diagnostics and therapy since the 1990s. Several different commercial products are available, such as SonoVue[1] and Optison,[2] that have been widely used for imaging of the heart, blood vessels, kidneys, and liver.[3] In 1999, Kripfgans et al discovered a phenomenon called acoustic droplet vaporization, where liquid-filled droplets are converted to gas-filled microbubbles by means of ultrasound exposure below a specific peak negative pressure.[4] This discovery has led to the development of phase-change contrast agents that have enabled novel clinical applications such as localized drug delivery, embolotherapy, oxygen delivery, photodynamic therapy, and histotripsy.[5–10] The liquid core of phase-changing contrast agents has an increased stability compared to gas-filled microbubbles during circulation in blood and during storage.[11] These droplets have the potential to act as drug delivery facilitators through stable and inertial cavitation induced by ultrasound.[12–14] However, the stability of phase-change contrast agents may be further improved to match the stability of solid core contrast agents.[15]

Paclitaxel is a hydrophobic molecule derived from Pacific yew *Taxus brevifolia* that was first approved by the US Food and Drug Administration for treatment of ovarian and breast cancer in 1992.[16–19] However, the drug's hydrophobicity makes efficient drug delivery of paclitaxel challenging.[20] In addition, commercial formulation of paclitaxel for intravenous administration is based on ethanol and Cremaphor EL (1:1) as solvent combination, which has been shown to

cause side effects such as hypersensitivity in patients.[16,21] Therefore, novel drug delivery systems that would increase the pharmaceutical efficiency of paclitaxel while decreasing the side effects are desirable.

Pickering emulsions, which are stabilized by solid particles instead of surfactants, were discovered at the beginning of the 20th century.[22,23] Pickering emulsions are much more stable than emulsions stabilized by surfactants due to the high desorption energies required to remove the particles from the interface between two immiscible liquids.[24] Liquid-filled capsules stabilized via a Pickering mechanism could further enhance the stability of phase change ultrasound contrast agents.

Recently, perfluoropentane (PFP) droplets stabilized by cellulose nanofibers (CNFs) were developed by Ghorbani et al.[11] The acoustic and mechanical properties of these droplets have been studied both in numerical and experimental studies;[25–27] however, the biological compatibility of these droplets is still unknown. The aim of this work was to study the effect of CNF-shelled PFP droplets on cancer cell viability, using murine breast cancer cell line 4T1 as a model. Firstly, thermal tests were performed to study how temperature affects the size distribution and concentration of CNF-shelled PFP droplets. Secondly, the impact of paclitaxel concentration and exposure time on 4T1 cell viability was investigated over a range of different concentrations. Thirdly, a hemolysis test was performed to investigate the in-blood safety of CNF-shelled PFP droplets. Finally, the effect of CNF-shelled PFP droplets with or without the presence of non-encapsulated paclitaxel on the cell viability was studied. This case study gives insight into the biocompatibility of CNF-shelled PFP droplets and provides the evidence to support their biological application.

Materials and Methods
Materials
Bleached sulfite pulp, kindly donated by Nordic Paper Seffle AB, Säffle, Sweden, was used for the production of CNFs. A 1.3 wt% cationic CNF suspension was manufactured from the bleached pulp as described elsewhere.[28,29] In short, the bleached sulfite pulp reacted with glycidyltrimethylammonium chloride (epoxypropyltrimethylammonium chloride) at a reaction temperature that was first gradually increased from 40°C to 50°C during 1 hour and then maintained at 50°C for 1 hour. A 0.35 wt% cationic CNF suspension was produced by diluting the 1.3 wt% stock suspension with Milli-Q water and sonicating it using a 1/2 in. tip and Sonics Vibracell W750 (Sonics and Materials Inc., Newton, CT, US) for 1 minute at 90% amplitude. PFP (99% purity) was purchased from Apollo Scientific (Stockport, United Kingdom). Paclitaxel (99.5+%) was purchased from Thermo Fisher Scientific (Massachusetts, US.).

Droplet Production
Droplets were manufactured using a similar approach as described elsewhere.[11] In short, 1 g of PFP was mixed with 36.1 g of 0.35 wt% cationic CNF suspension (pH of CNF suspension was 10.5) via mechanical agitation. The suspension was mixed using an Ultra-Turrax (IKA Werke GmbH, Staufen, Germany) in combination with a 25 N - 8 G Dispersing Tool which was used for 90 seconds at maximum speed (~25,000 rpm). After production, the mother droplet suspension was diluted in Milli-Q in 1:4 ratio and centrifuged at 1000 rpm for 5 minutes. Lastly, the supernatant was removed and Milli-Q water added. A schematic illustration showing the droplet production process is presented in Figure 1.
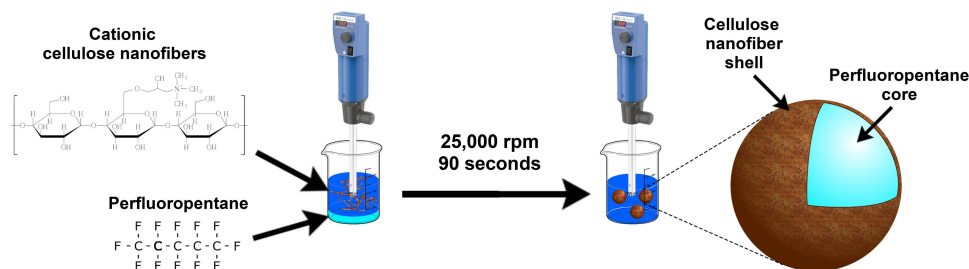
Figure 1 A schematic illustration of droplet production.

Droplet Characterization

Optical Microscopy

The number and volume size distributions and concentration were determined by using an optical microscope (Eclipse Ni-E, Nikon Corporation, Japan) and a sCMOS Andor Zyla 4.2 camera (Andor Instruments, Belfast, UK). The droplets were introduced into a Neubauer counting chamber and left to form sediment for 25 minutes before imaging to allow for droplets and potential gas-filled bubbles to separate to different imaging planes. The volume size distribution and concentration of droplets were calculated based on droplets located at the bottom of the Neubauer counting chamber. A 10x magnification objective (Nikon Corporation, Japan) was used when measuring the concentration, and a 20x magnification objective (Nikon Corporation, Japan) for determining the volume size distribution. Images were later processed using Fiji software (v1.53q),[30] and the final figures and data were calculated using an in-house Matlab script. The polydispersity index (PDI) for each sample of CNF-shelled PFP droplets was calculated from the number size distribution as the ratio between the standard deviation of the droplet diameter distribution σ and mean diameter D squared:

$$PDI = \left(\frac{\sigma}{D}\right)^2$$

Field Emission Scanning Electron Microscopy (FESEM)

A drop of the centrifuged suspension of CNF-shelled PFP droplets was dropped on top of Si wafers, allowed to dry at ambient conditions in the room, and lastly spur-coated (Cressington 208HR sputter coater) with a Cr coating for 60 seconds prior to imaging. A Hitachi SEM S-4800 (Japan) at an accelerating voltage of 1 kV was used.

Fourier-Transform Infrared Spectroscopy (FTIR)

Fourier-transform infrared spectroscopy (FTIR) spectra were obtained for 0.35 wt% CNF suspension and CNF-shelled PFP droplets using a PerkinElmer Spectrum 100 instrument equipped with an ATR accessory. A drop of each sample was put on a cover glass and dried at 40°C for at least 24 hours before measurement. Then, the dried sample was scraped off using a scalpel and put in the instrument. The measurements were performed at a scanning rate of 1 cm^{-1} at a resolution of 4 cm^{-1}. The absorbance was measured 16 consecutive times between 600 and 4000 cm^{-1}. All measurements were performed at room temperature (~22°C).

Thermal Tests

The volume size distribution and concentrations of droplets at temperatures relevant for cell studies were tested and compared to the volume size distribution and concentration at room temperature (~22°C). Droplets were produced and stored in the refrigerator at 8°C for 24 hours. Afterwards, the sample was divided into two vials: one that was left at room temperature, and one that was put in an incubator at 37°C. The host medium during the thermal tests was MilliQ water. The volume size distribution and concentration before and after the thermal exposure were measured and analyzed according to the scheme described earlier in this manuscript. In addition, images were taken of the mother suspension immediately after production, 24 hours after production, and 72 hours after production, respectively. The times were chosen to correspond to time points in cell viability tests.

Cell Culture

Triple negative murine breast cancer cells 4T1 were purchased from ATCC (Catalog No. CRL-2539) and cultured in RPMI 1640 (Gibco; Catalog No. 72400) supplemented with 10% fetal bovine serum (FBS; ThermoFisher; Catalog No. 10500064) and 1% penicillin (100 U/mL)-streptomycin (0.1 mg/mL) (Sigma-Aldrich; Catalog No. P4333) at 5% CO_2 under 37°C. Cells with passage number ≤ 10 were used for the subsequent experiments.

Hemolysis Assay

Hemolysis assay was performed to evaluate blood compatibility. Mouse whole blood was collected by cardiac puncture and stabilized. 2 mL of whole blood sample was diluted with 4 mL phosphate-buffered saline (PBS) and red blood cells

(RBCs) were isolated after centrifugation at 10,000 *g* for 5 min. After washing five times with 10 mL PBS, the RBCs were resuspended with 20 mL PBS. 0.2 mL RBC suspension was mixed with 0.8 mL of the droplets PBS suspension at a concentration of 300, 600, 900 droplets/mL to make the final droplets concentration 240, 480, 720 droplets/mL, distilled water was positive group, and PBS was negative group. Every group had four repeats. After incubation at room temperature for 4 h and centrifugation for 5 min at 10,000 *g*, 100 µL of the supernatant was transferred to a 96-well plate and the absorbance was measured by a microplate reader at 577 nm with 655 nm as a reference. The hemolysis % was calculated using the following formula:

$$\text{Hemolysis ratio} = (\text{OD}_{\text{test}} - \text{OD}_{\text{negative control}})/(\text{OD}_{\text{positive control}} - \text{OD}_{\text{negative control}}) \times 100\%$$

Cell Viability

The effect of paclitaxel, droplets, and a combination of them on 4T1 cells was determined through cell viability tests. The cells were then counted using Trypan Blue and a Bürker counting chamber and resuspended in cell medium at a cell density of 5.0×10^4 cells/mL. Finally, 100 µL cell suspension containing 5.0×10^3 cells/well were seeded in a 96-well plate (Corning Costar, USA).

Firstly, the effect of varying drug concentrations and exposure times was studied. For this, dimethyl sulfoxide (DMSO) dissolved paclitaxel was further diluted in cell culture medium at the final concentrations of 100 nM, 50 nM, 25 nM, 12.5 nM, 6.25 nM, 3.125 nM, and 1.56 nM, respectively. The cells were exposed to paclitaxel at different concentrations for 24 and 48 hours. To measure cell viability, the cell medium was removed and 10 µL of a 3-[4,5-dimethylthiazol-2yl]-2,5-diphenyltetrazolium bromide (MTT) reagent (5 mg/mL) was added to each well, left to react for 4 hours, and carefully removed. 100 µL of DMSO was added to each well to dissolve the formazan, and after 10 minutes' shaking the absorbance was measured at 570 nm using a spectrophotometer (SpectraMax i3x, Molecular Devices, CA, USA). The absorbance values were normalized in relation to the mean absorbance values of the control group without paclitaxel treatment.

Secondly, the effect of droplets on 4T1 cell viability without the addition of paclitaxel was studied. The number of droplets added to each well was chosen to be such that the total volume of these droplets would be equal to the volume of paclitaxel added to reach 50 nM working concentration in 100 µL. The molar volume of paclitaxel is 610.5 mL,[31] and therefore the drug volume per well was 3.05 pL. The number of droplets that was added to each cell well was chosen so that it would be similar to the volume taken up by paclitaxel. Therefore, 24 droplets were added per well. In addition, the double (48 droplets per well) and triple (72 droplets per well) amount of that was also studied to see whether an increased number of droplets would affect the cell viability.

Lastly, a combination of droplets and non-encapsulated paclitaxel was investigated to study any potential interaction on 4T1 cell viability. DMSO vehicle group was included as control. 48 hours after treatment, cell viability was measured using MTT assay as described previously.

Statistical Analysis

RStudio (Version 1.4.1106, Posit), an open-source software for statistical analysis, was used for statistical analysis of data. After thermal tests, statistical analysis was performed on data-points for number size distribution. Shapiro–Wilk test was chosen to test for normality. If the data did not follow a Gaussian distribution according to the Shapiro–Wilk test (ie, if the null hypothesis was rejected), an unpaired Wilcoxon test was performed to determine whether the samples of different groups were equal. Three comparisons were made: droplets at room temperature before and after exposure, droplets at 37°C before and after exposure, and droplets after exposure to room temperature or 37°C. An unpaired test was chosen, as we did not track the size of individual droplets, but rather of the two samples as a whole. A significance level of 0.05 was chosen for all tests.

For cell viability data, a linear regression model was applied to investigate the effect of concentration of droplets X_1, presence or absence of paclitaxel X_2, and their potential interaction $X_1{:}X_2$ on cell viability Y:

$$Y = \beta_0 + \beta_1 X_1 + \beta_2 X_2 + \beta_3 X_1{:} X_2 + \varepsilon$$

where ε is the estimated error of the function. First, the regression analysis was performed on original data. To accommodate for potential nonlinear effect, the model was also run where the different concentrations of CNF-shelled PFP droplets were considered as factors instead of continuous variables. These two analyses were performed both before

and after rank transformation of the measured absorbance values, as recommended by Conover.[32] In total, four tests were performed: ordinary linear regression, droplet concentration considered as a factor variable, rank transformation performed on cell viability data, and rank transformation in combination with droplet concentration considered as a factor variable. The influence of DMSO on 4T1 cell viability was tested using an unpaired Wilcoxon test. A significance level of 0.05 was chosen for all tests.

Results

Droplet Characterization

The surface morphology of CNF-shelled PFP droplets was examined using FESEM. Figure 2A shows the FESEM image that displays individual fibers on the surface of collapsed droplets. The FTIR spectra of neat CNF and CNF-shelled PFP droplets is presented in Figure 2B and C. Two bands were observed for both samples at 3340 and 2890 cm^{-1}, corresponding to the stretching vibration of O-H and asymmetric stretching vibration of C-H, respectively.[33] The band of CNF (red) and CNF-shelled PFP droplets (blue) at around 1050 correspond to pyranose ring ether band of cellulose,[34] and is similar to previous work by Svagan et al utilizing the same CNF.[28] The new band present in the spectrum of CNF-shelled PFP droplets (blue) between 1100 and 1300 cm^{-1} compared to the pure CNF spectrum is due to PFP.[35,36]

Thermal Tests

Droplet stability was studied during storage in refrigerator (8°C), at room temperature (~22°C), and at a physiologically relevant temperature (37°C). In addition, the mother suspension (non-centrifuged) kept in the refrigerator at 8°C was photographed immediately after droplet production, and after 24 and 72 hours. The images of the mother suspension are presented in Figure 3.

As can be seen in Figure 3A, immediately after production the suspension was completely homogenous, with only a few larger bubbles present. After 24 hours, a foam started to form on top of the suspension, containing many gas-filled bubbles with diameters of several millimeters. The foam increased in size over time, with an increase of both the size of the bubbles and the number of bubbles, as can be seen in Figure 3C.

The volume size distribution and concentration of CNF-shelled PFP droplets were investigated by using an optical microscope and a Neubauer counting chamber. Images were taken at two imaging planes to study whether droplets formed sediment at the bottom of the chamber or not. As shown in Figure 4, most of the droplets were located in the same focus plane as the grid, thus they did form sediment. However, some individual droplets did float at a higher imaging plane even after the sample was left for 25 minutes after injection into the chamber (Figure 4B).
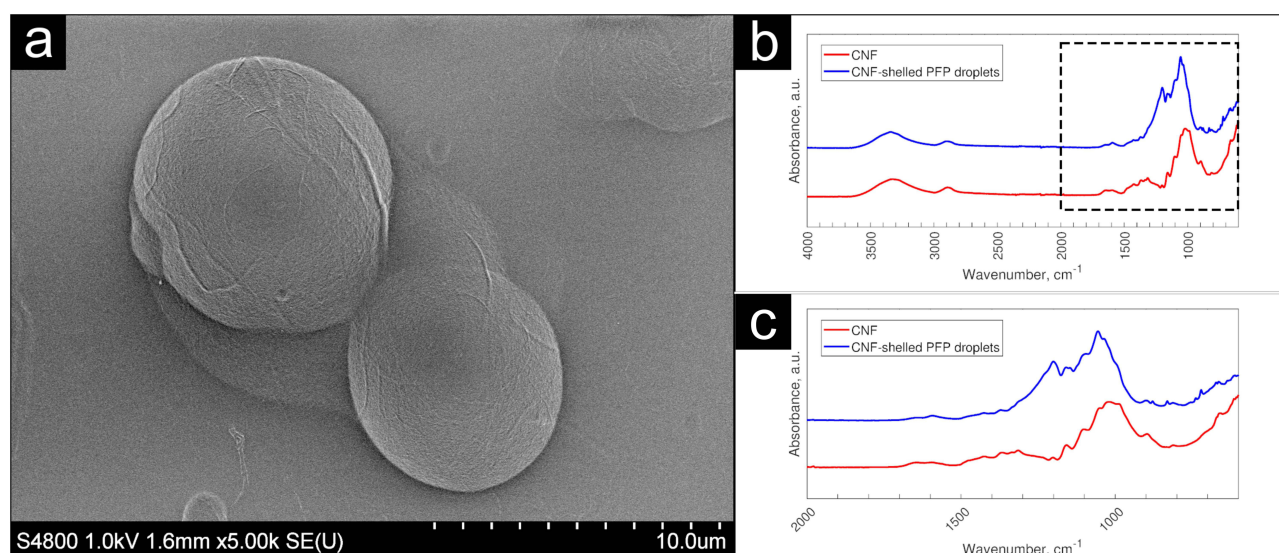
Figure 2 (**A**) An FESEM image of collapsed CNF-shelled PFP droplets; (**B**) full FTIR spectrum of dried CNF and CNF-shelled PFP droplets, and (**C**) zoomed-in FTIR spectrum between 600 and 2000 cm^{-1}.
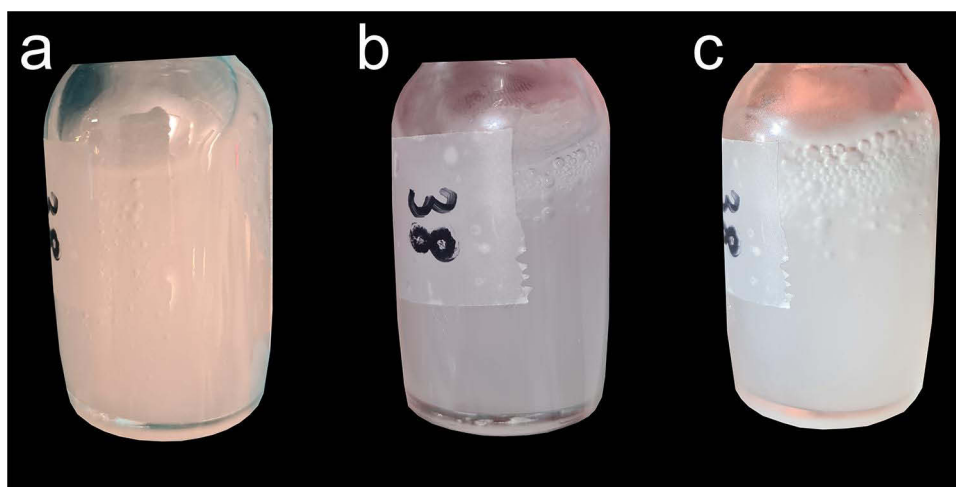
Figure 3 Droplet suspension (not centrifuged) (**A**) immediately after production, (**B**) 24 hours and (**C**) 72 hours after production. A visible foam formed on top of the suspension, showing coalescing in the suspension.
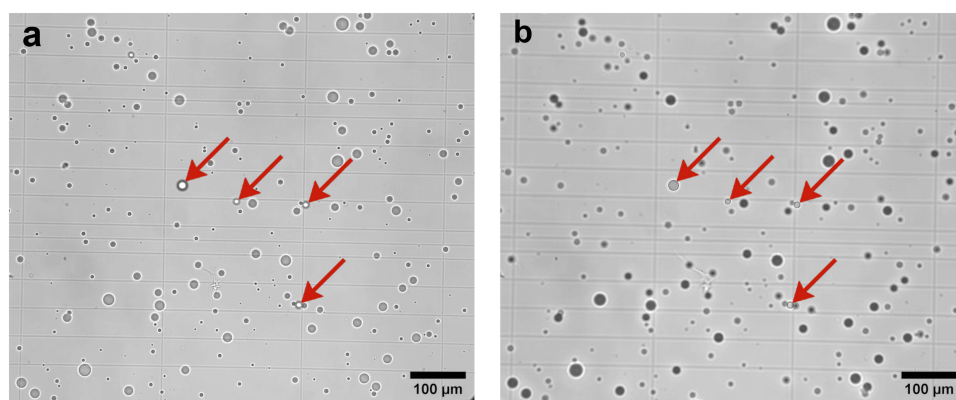
Figure 4 Droplets in the Neubauer counting chamber 25 minutes after introduction. (**A**) Most of the droplets are in the same imaging plane as the grid, signifying that they are located at the bottom of the chamber, but (**B**) some droplets (marked with red arrows) are located at a higher imaging plane.

The volume size distribution and concentration of droplets were calculated based on droplets located at the bottom of the Neubauer counting chamber. The concentration was the same for both groups before the measurement started ($3.65 \pm 0.29 \times 10^6$ droplets/mL and $3.50 \pm 0.64 \times 10^6$ droplets/mL at room temperature and in the incubator, respectively). The concentration decreased after 48 hours for both groups, but it decreased more for droplets stored at 37°C ($1.94 \pm 0.10 \times 10^6$ droplets/mL) compared to droplets stored at room temperature ($2.56 \pm 0.22 \times 10^6$ droplets/mL). It is worth noting that more than half of the initial droplets were still observed after 48 hours in both groups.

The number and volume size distributions for droplets are presented in Figure 5 and Table 1. The number of droplets included in the measurement of size distributions before and after exposure to room temperature for 48 hours was 1601 and 1057, respectively. At 37°C, the number of droplets that were included in the measurement before and after exposure was 1387 and 684, respectively. The droplet size decreased after 48 hours for both groups. For droplets exposed to room temperature, the average volume diameter decreased from 15.0 ± 5.5 μm to 13.6 ± 5.6 μm; for droplets in the incubator at 37°C, the size changed from 14.4 ± 5.3 μm to 12.8 ± 4.9 μm. The corresponding change in PDI, calculated from the number size distribution for each sample at room temperature and at 37°C was from 0.41 to 0.35 and from 0.39 to 0.38, respectively. The Shapiro–Wilk test showed that the size distribution data did not have a Gaussian distribution at any temperature nor time-point. The decrease in droplet diameter was statistically significant at both room temperature ($p = 0.01415 < 0.05$) and at 37°C ($p = 0.002713 < 0.05$). However, there was no statistically significant difference in size distributions after 48 hours ($p = 0.2063 > 0.05$).

1840

International Journal of Nanomedicine 2023:18
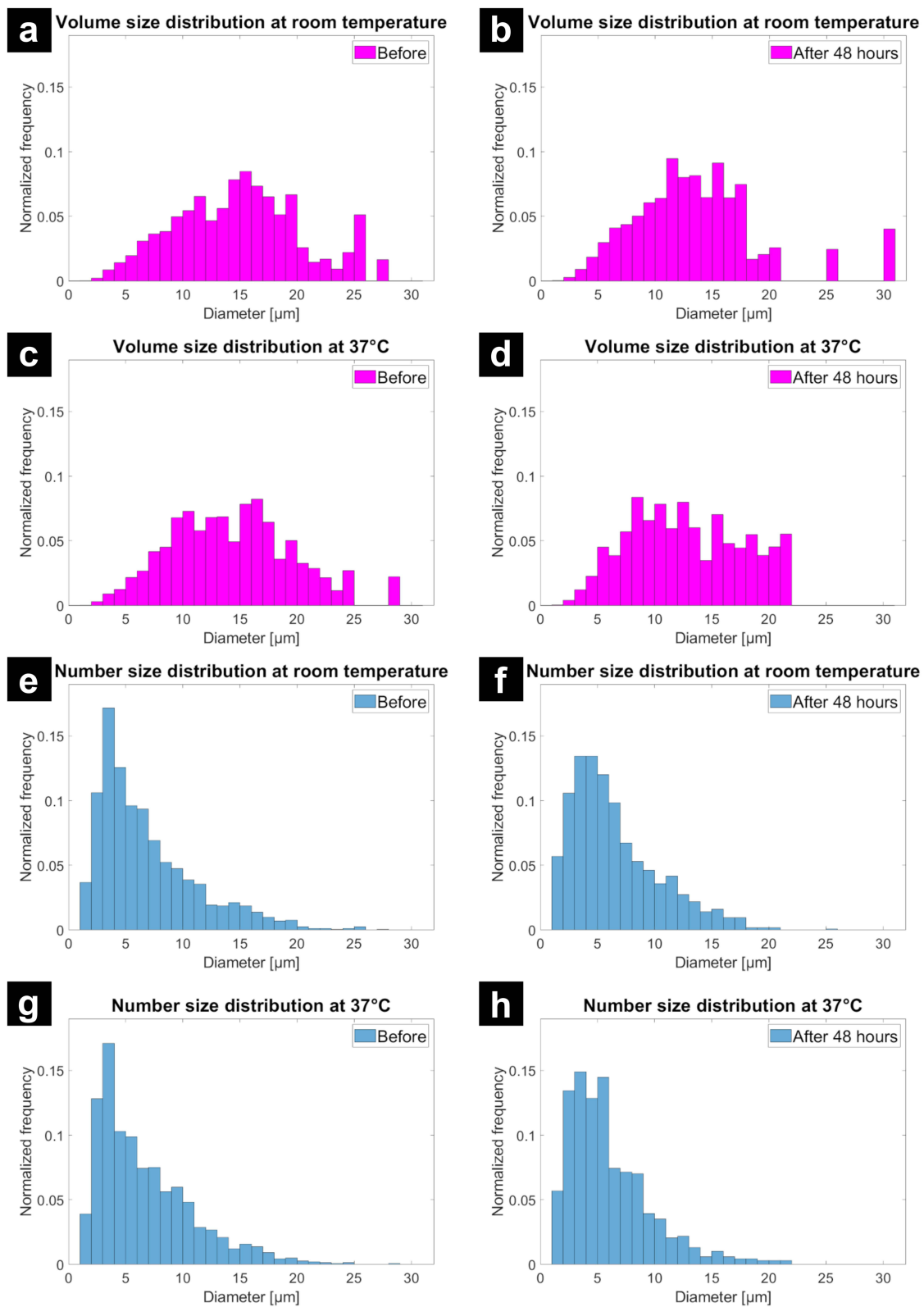
Figure 5 The volume size distribution of CNF-shelled PFP droplets (**A**) at room temperature before and (**B**) at room temperature after 48 hours of exposure, and (**C**) at 37°C before and (**D**) at 37°C after 48 hours of exposure. In addition, the number size distribution of CNF-shelled PFP droplets is presented: (**E**) at room temperature before exposure, and (**F**) at room temperature after 48 hours; (**G**) at 37°C before, and (**H**) at 37°C after 48 hours of exposure.

Table 1 The Number and Volume Size Distributions of CNF-Shelled PFP Droplets Exposed to Room or Physiological Temperature (22 or 37°C, respectively). The Numbers Presented Here are the Mean and Standard Deviation for Each Size Distribution

	Number Size Distribution		Volume Size Distribution	
	Before	After 48 Hours	Before	After 48 Hours
Room temperature	6.9 ± 4.4 µm	6.6 ± 3.9 µm	15.0 ± 5.5 µm	13.6 ± 5.6 µm
37°C	6.7 ± 4.2 µm	6.0 ± 3.7 µm	14.4 ± 5.3 µm	12.8 ± 4.9 µm

Abbreviations: CNF, cellulose nanofibers; PFP, perfluoropentane; MTT, 3-[4,5-dimethylthiazol-2yl]-2,5-diphenyltetrazolium bromide; DMSO, dimethyl sulfoxide; FESEM, field emission scanning electron microscopy; FTIR, Fourier-transform infrared spectroscopy; RBC, red blood cell; PBS, phosphate-buffered saline.

Biocompatibility

Figure 6 presents the results from hemolysis assay and 4T1 cell viability tests. As can be seen in Figure 6A, only the positive control (water) caused significant hemolysis of RBCs. The effects of paclitaxel, DMSO, and droplets on cell viability of 4T1 cells were studied (Figure 6B-E). As shown in Figure 6B, the cell viability decreased when paclitaxel concentration increased from 1.56 nM to 100 nM. In addition, the cell viability was lower at all concentrations except the two lowest concentrations after 48 hours' treatment compared to 24 hours' treatment. No significant cell toxicity was observed in DMSO vehicle group (Figure 6C) at 48 hours, which contained equal amount of DMSO as 100 nM paclitaxel treatment group. Four different linear regression models were applied to the 4T1 cell viability data to investigate the effects of CNF-shelled PFP droplets, paclitaxel, and any potential interactions between them. Only paclitaxel showed a statistically significant influence on 4T1 cell viability with a decrease of 38% compared to the control, as can be seen in Figure 6E. No further decrease in cell viability was observed when CNF-shelled PFP droplets were added in addition to paclitaxel at any concentration. Without the addition of paclitaxel, 4T1 cell viability increased at the lowest droplet concentration of 24 droplets per well compared to the control group ($p = 0.0443 < 0.05$) when droplet concentration was considered a factor variable; however, this increase was no longer statistically significant after rank transformation ($p = 0.132 > 0.05$). Thus, it can be concluded that CNF-shelled PFP droplets did not have an effect on 4T1 cell viability at any concentration.

Discussion

Thermal tests were performed to study the change in volume size distribution of droplets over time at different temperatures. Previous studies have shown that CNF-shelled PFP droplets are stabilized via a Pickering mechanism.[11] Figure 2A shows that similarly to the previous work by Ghorbani et al[11] and Loskutova et al,[27] CNFs act as a stabilizing agent as they form a coherent layer on the surface of the droplets. The initial droplet size of the produced emulsion is determined by the energy density, ie, energy dissipated per unit volume of the processed mixture, with an increase in energy output decreasing the size of produced droplets.[37–40] Abismaïl et al showed that the droplet size was significantly smaller when an ultrasound homogenizer was used compared to an Ultra-Turrax due to less heat loss.[38] A similar trend was observed by Wang et al when oil-in-water emulsions were prepared by either low-energy Ultra-Turrax or a high-pressure homogenizer,[41] which is another high-energy method for emulsification similar to an ultrasonic homogenizer.[42] This is in line with our observations, as CNF-shelled PFP droplets produced by Ultra-Turrax had a larger diameter than droplets developed by Ghorbani et al who utilized ultrasonication for mixing.[11] The foam formation as shown in Figure 3 was not observed when CNF-shelled PFP droplets were produced by ultrasonication in a previous study, where droplets remained stable for up to a month.[11] Kalashnikova et al showed that Pickering emulsions with cellulose nanocrystals as stabilizing particles could be stable even for several months.[43] The foam formation in CNF-shelled PFP droplets produced by Ultra-Turrax may be due to less homogenous dispersion of the CNFs during production compared to if ultrasonication was used, resulting in a lower surface coverage and decreased emulsion stability. In addition, previous work has shown that the size and stability of Pickering emulsions are dependent on the size of the stabilizing particle.[44–46] Lee et al showed that the fiber size of TEMPO-oxidized
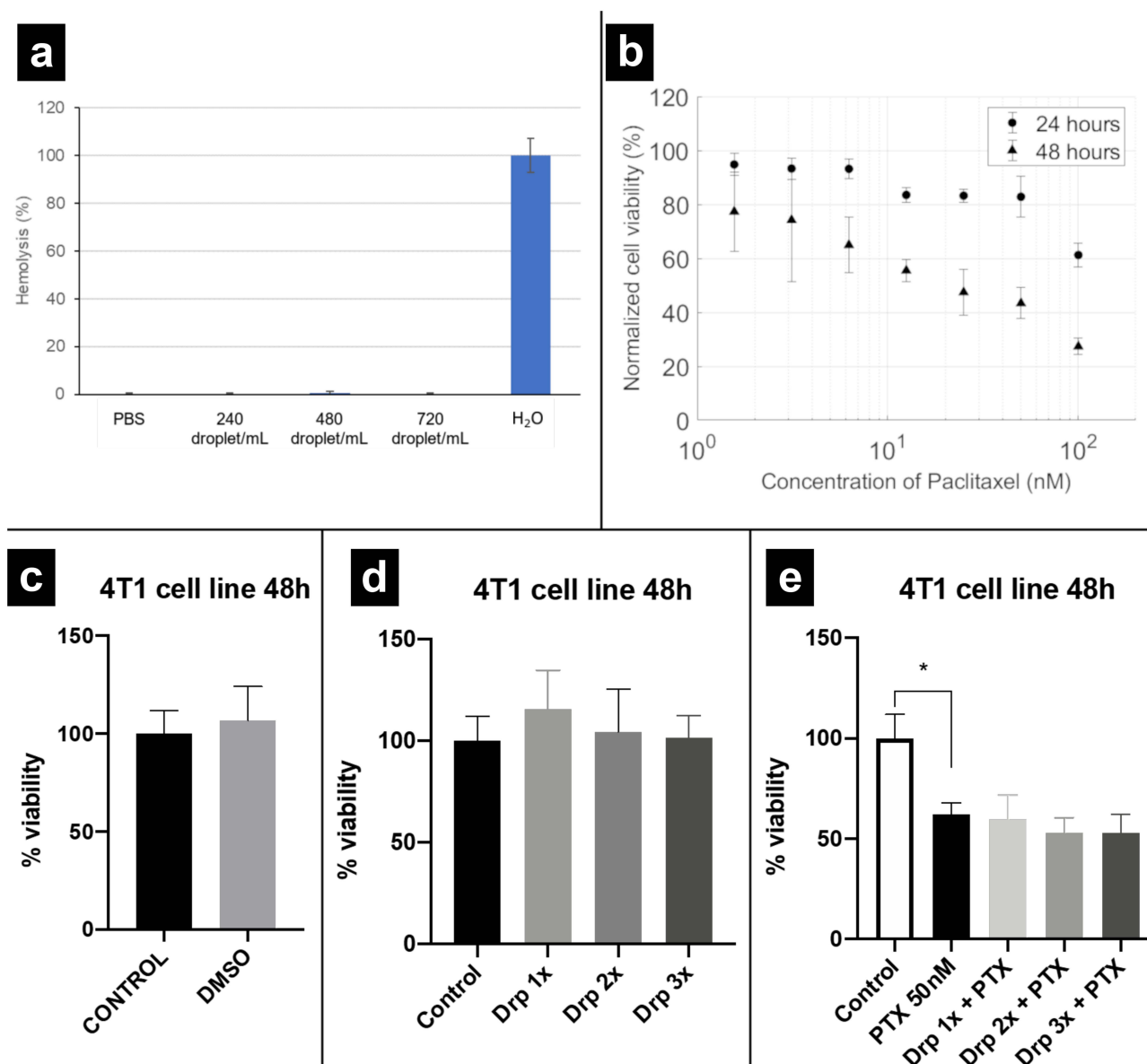
Figure 6 (**A**) Hemolysis ratio after exposure to positive control (PBS), negative control (water) or CNF-shelled PFP droplets. Only negative control caused visible hemolysis. (**B-E**) Cell viability of 4T1 cells when studying the effect of (**B**) paclitaxel concentration and exposure time; (**C**) DMSO; (**D**) presence of droplets (where 1x, 2x and 3x are equal to 24, 48 and 72 droplets per well, respectively); and (**E**) combination of droplets and drug in each well. The cell viability decreased from 100% to 62% ± 6% in 50 nM paclitaxel treatment group; however, no additional significant decrease in cell viability was observed when CNF-shelled droplets were added. * $p < 0.05$.

CNF decreased with increased sonication time of the fibers.[47] This indicates that the CNF particles in this study could be larger than when ultrasonication was used by Ghorbani et al,[11] decreasing their stabilizing properties.

When thermal tests were performed on droplets in this study, it was observed that the droplet diameter decreased with increasing temperature after 48 hours (Figures 5A-D). While the size distribution and polydispersity of the sample produced by Ghorbani et al increased with increasing temperature,[11] CNF-shelled PFP droplets produced in this study had the opposite effect. The decrease in size observed in Figures 5A-D is due to coalescence and later collapse of larger droplets, whilst smaller droplets with a diameter of below 15 μm remained in the sample. After droplets' collapse, PFP is evaporated due to the low boiling temperature at ambient pressure (29°C).[5] This can be supported by the decrease in droplet concentration observed at both room temperature and 37°C, and a more significant decrease when droplets were exposed to a higher temperature.

As the average diameter of a droplet was determined to be between 14.4 and 15.0 μm (Figure 5), the average volume of a droplet is between 1.56 and 1.77 pL. Therefore, 24, 48, and 72 droplets per well correspond to a total volume of 37.44 to 42.48, 74.88 to 84.96, and 112.32 to 127.44 pL, respectively. This is 12 to 42 times higher than the volume taken up by the paclitaxel when a 50 nM solution is added to the cell well.

The effect of paclitaxel, droplets and a combination of both on 4T1 cell viability were studied. As can be seen in Figure 6B, cell viability of 4T1 cells decreased with increasing drug concentration from 1.56 to 100 nM. Additionally, cell viability was lower after 48 hours compared to an exposure time of 24 hours, with the exception of the two lowest concentrations of 1.56 and 3.125 nM. The cell viability was always above 60% even at the highest concentration of paclitaxel, but with a longer exposure time the cell viability decreased to as low as 27%. The half maximal inhibitory concentration IC_{50} was between 12.5 and 25 nM at an exposure time of 48 hours, as can be seen in Figure 6B. Previous studies have shown that IC_{50} of paclitaxel on 4T1 cells was between 2.06 and 43 μM if the exposure time was 8 hours.[48–50] In the work conducted by Liebmann et al, IC_{50} decreased to between 2.5 and 7.5 nM for HeLa, A549, MCF-7, U373, and HT-29 cell lines when the exposure time was increased to 24 hours.[51] This trend was also observed by Georgiadis et al, with the IC_{50} decreasing as the exposure time increased when the cytotoxicity of paclitaxel was tested in vitro on 28 human lung cancer cell lines.[52] Worth noting is that Liebmann et al showed that non-proliferating cells were markedly more resistant to paclitaxel than cells growing exponentially.[51] The reason for this is that paclitaxel works by stabilizing the microtubules and blocking the cell cycle, thus causing cell death.[16]

Many different parameters can influence the toxicity of micro- and nanodroplets, such as material properties, shape, size, and phase of the core. The two droplet components that may have a cytotoxic effect is the cationic CNFs and PFP. Previous studies have estimated the volume fraction of CNF to be between 1.5% and 8.8%[27] and the density of CNFs to be 1.5 g/cm^3.[53] Therefore, the volume of CNF present in 72 droplets should be between 1.68 and 11.21 pL, or between 2.53 and 16.82 ng. Since the volume in each well was 100 μL, this gives a maximum CNF concentration of between 25.3 and 168.2 ng/mL. Both the maximum concentration of CNF present in our solution and the total volume of the droplets was low, which should be taken into account when considering the possible effect on cell viability.

PFP has been extensively used as core material in drug carriers for ultrasound-mediated drug delivery as it is biocompatible and biodegradable.[5,11,54,55] CNF, on the other hand, has shown different levels of toxicity depending on the concentration of fibers, particle size and shape, and surface charge and chemistry.[56] Čolić et al reported that non-chemically treated CNFs did not induce any cytotoxicity or oxidative stress at any concentration of CNFs (31.25 μg/mL – 1 mg/mL) for L929 cells, nor induced necrosis or apoptosis in thymocytes and human peripheral blood mono-nuclear cells.[57] When the effect of surface modification of wood-derived CNFs on three different cell types (human dermal fibroblasts, lung MRC-5 cells and THP-1 macrophage cells) was studied by Lopes et al, the results showed that there was no cytotoxic effect associated with the exposure to unmodified, carboxymethylated and hydroxypropyltri-methylammonium-modified nanofibrillated cellulose.[58] Malmir et al and Abolghasemzade et al showed that bacterial cellulose could even be used in nanocomposites in combination with carbon quantum dots and titanium dioxide nanoparticles, or carbon quantum dots, silica nanoparticles, and silk fibroin, respectively, due to its low cytotoxicity and antibacterial properties.[59,60] However, it is important to note that the focus of this study is the potential toxic impact of CNF-shelled droplets and not individual fibers, and therefore other aspects also need to be taken into account, such as influence from droplet shape and size, and the physical characteristics of the droplet core material.

The morphology of the droplet might affect the cytotoxicity in comparison to individual fibers, as immune cells respond differently depending on the size and shape of the foreign object.[61] The average tumor cell diameter is between 10 and 25 μm, as determined by Hosokawa et al,[62] which is in the same order of magnitude as the CNF-shelled PFP droplets. Therefore, the cells most probably encounter a curved surface, which is something in-between individual fibers and a flat cellulose film. Basti et al showed that hydrogels constructed from hydroxyethyl cellulose and citric acid crosslinker were non-toxic to NIH-3T3 cells after 1 and 3 days of exposure.[63] Similar results were obtained by Ezati et al, who showed that functional CNF-based films prepared by incorporating two types of carbon dots were non-toxic to L929 cells after 72 h treatment.[64] The results from these studies suggest that even if CNFs are in contact with a larger area of the cell, the effect on cell viability is limited.

Different drug carriers and ultrasound contrast agents have been developed over the years with both gas and liquid core. However, previous works have shown that drug carriers and contrast agents are only influencing the biological activity of the cell (ie, inducing apoptosis, or decreasing cell viability) after ultrasound exposure.[13,14,65,66] The reason for the biological effects is the mechanical and cavitation damage to cell membrane produced by either the acoustically activated microbubbles, phase-change nanodroplets or the ultrasound itself. Grishenkov et al showed that polyvinyl alcohol-shelled microbubbles loaded with nitric oxide were phagocytosed by macrophages after 6 hours of incubation, and that microbubbles do not influence the cell viability of macrophages.[65] This is also in line with other work.[67]

Conclusion

In summary, CNF-shelled PFP droplets were produced by mixing, using Ultra-Turrax. The thermal effect on volume size distribution and concentration of these droplets was tested, and the effect on cell viability of 4T1 cells was determined by an MTT assay. CNF-shelled PFP droplets showed increased signs of instability after 24 and 48 hours due to non-homogenous dispersion of CNFs and their decreased ability to stabilize the PFP-water interface compared to similar droplets produced by ultrasonication. The droplet diameter and concentration of CNF-shelled droplets decreased with increasing temperature, as these factors influence the vaporization threshold of the liquid PFP core. The cell viability of 4T1 cells decreased with increasing exposure time and concentration of paclitaxel. The CNF-shelled PFP droplets had no influence on the cell viability of 4T1 cells, and no additional influence on the cell viability when paclitaxel was also added to the cells. These results indicate that CNF-shelled PFP droplets have potential as a drug carrier in ultrasound-mediated therapy.

Acknowledgments

Disclosure

The authors report no conflicts of interest in this work.

References

1. Bokor D. Diagnostic efficacy of SonoVue. *Am J Cardiol*. 2000;86(4):19–24. doi:10.1016/s0002-9149(00)00985-1
2. Cohen JL, Cheirif J, Segar DS, et al. Improved left ventricular endocardial border delineation and opacification with OPTISON (FS069), a new echocardiographic contrast agent - Results of a Phase III multicenter trial. *J Am Coll Cardiol*. 1998;32(3):746–752. doi:10.1016/S0735-1097(98)00311-8
3. Cosgrove D, Harvey C. Clinical uses of microbubbles in diagnosis and treatment. *Med Biol Eng Comput*. 2009;47(8):813–826. doi:10.1007/s11517-009-0434-3
4. Kripfgans OD, Fowlkes JB, Miller DL, Eldevik OP, Carson PL. Acoustic droplet vaporization for therapeutic and diagnostic applications. *Ultrasound Med Biol*. 2000;26(7):1177–1189. doi:10.1016/S0301-5629(00)00262-3
5. Loskutova K, Grishenkov D, Ghorbani M. Review on Acoustic Droplet Vaporization in Ultrasound Diagnostics and Therapeutics. *Biomed Res Int*. 2019;2019. doi:10.1155/2019/9480193
6. Wu SY, Fix SM, Arena CB, et al. Focused ultrasound-facilitated brain drug delivery using optimized nanodroplets: vaporization efficiency dictates large molecular delivery. *Phys Med Biol*. 2018;63(3). doi:10.1088/1361-6560/aaa30d
7. Krafft MP, Riess JG. Therapeutic oxygen delivery by perfluorocarbon-based colloids. *Adv Colloid Interfac*. 2021;294:102407. doi:10.1016/j.cis.2021.102407
8. Xavierselvan M, Cook J, Duong J, Diaz N, Homan K, Mallidi S. Photoacoustic nanodroplets for oxygen enhanced photodynamic therapy of cancer. *Photoacoustics*. 2022;25:100306. doi:10.1016/j.pacs.2021.100306
9. Harmon JS, Kabinejadian F, Seda R, et al. Minimally invasive gas embolization using acoustic droplet vaporization in a rodent model of hepatocellular carcinoma. *Sci Rep-Uk*. 2019;9. doi:10.1038/s41598-019-47309-y
10. Khirallah J, Schmieley R, Demirel E, et al. Nanoparticle-mediated histotripsy (NMH) using perfluorohexane 'nanocones'. *Phys Med Biol*. 2019;64(12):125018. doi:10.1088/1361-6560/ab207e
11. Ghorbani M, Olofsson K, Benjamins J-W, et al. Unravelling the Acoustic and Thermal Responses of Perfluorocarbon Liquid Droplets Stabilized with Cellulose Nanofibers. *Langmuir*. 2019;35(40):13090–13099. doi:10.1021/acs.langmuir.9b02132
12. Roovers S, Segers T, Lajoinie G, et al. The Role of Ultrasound-Driven Microbubble Dynamics in Drug Delivery: from Microbubble Fundamentals to Clinical Translation. *Langmuir*. 2019;35(31):10173–10191. doi:10.1021/acs.langmuir.8b03779

13. Qin HC, Teng R, Liu Y, Li J, Yu M. Drug Release from Gelsolin-Targeted Phase-Transition Nanoparticles Triggered by Low-Intensity Focused Ultrasound. *Int J Nanomed*. 2022;17:61–71. doi:10.2147/Ijn.S341421

14. Zhou J, Hou JX, Liu SL, et al. Theranostic Nanoplatform with Sequential SDT and ADV Effects in Response to Well-Programmed LIFU Irradiation for Cervical Cancer. *Int J Nanomed*. 2021;16:7995–8012. doi:10.2147/Ijn.S339257

15. Tarighatnia A, Fouladi MR, Nader ND, Aghanejad A, Ghadiri H. Recent trends of contrast agents in ultrasound imaging: a review of the classifications and applications. *Mater Adv*. 2022;3(9):3726–3741. doi:10.1039/d1ma00969a

16. Alves RC, Fernandes RP, Eloy JO, Salgado HRN, Chorilli M. Characteristics, Properties and Analytical Methods of Paclitaxel: a Review. *Crit Rev Anal Chem*. 2018;48(2):110–118. doi:10.1080/10408347.2017.1416283

17. Wani MC, Taylor HL, Wall ME, Coggon P, McPhail AT. Plant antitumor agents. VI. The isolation and structure of taxol, a novel antileukemic and antitumor agent from Taxus brevifolia. *J Am Chem Soc*. 1971;93(9):2325–2327. doi:10.1021/ja00738a045

18. McGuire WP, Rowinsky EK, Rosenshein NB, et al. Taxol - a Unique Antineoplastic Agent with Significant Activity in Advanced Ovarian Epithelial Neoplasms. *Ann Intern Med*. 1989;111(4):273–279. doi:10.7326/0003-4819-111-4-273

19. O'Shaughnessy JA, Cowan KH. Current status of paclitaxel in the treatment of breast cancer. *Breast Cancer Res Treat*. 1995;33(1):27–37. doi:10.1007/BF00666068

20. Ezrahi S, Aserin A, Garti N. Basic principles of drug delivery systems - the case of paclitaxel. *Adv Colloid Interfac*. 2019;263:95–130. doi:10.1016/j.cis.2018.11.004

21. Kingston DGI. The shape of things to come: structural and synthetic studies of taxol and related compounds. *Phytochemistry*. 2007;68(14):1844–1854. doi:10.1016/j.phytochem.2006.11.009

22. Ramsden W. Separation of solids in the surface-layers of solutions and 'suspensions'(observations on surface-membranes, bubbles, emulsions, and mechanical coagulation).—Preliminary account. *Proce Royal Soc London*. 1904;72(477–486):156–164. doi:10.1098/rspl.1903.0034

23. Pickering SU. CXCVI.—Emulsions. *J Chemical Soc Transactions*. 1907;91:2001–2021. doi:10.1039/CT9079102001

24. Binks BP, Lumsdon SO. Pickering Emulsions Stabilized by Monodisperse Latex Particles: effects of Particle Size. *Langmuir*. 2001;17(15):4540–4547. doi:10.1021/la0103822

25. Song X, Loskutova K, Chen HJ, Shen GF, Grishenkov D. Deriving acoustic properties for perfluoropentane droplets with viscoelastic cellulose nanofiber shell via numerical simulations. *J Acoust Soc Am*. 2021;150(3):1750–1761. doi:10.1121/10.0006046

26. Loskutova K, Nimander D, Gouwy I, et al. A Study on the Acoustic Response of Pickering Perfluoropentane Droplets in Different Media. *ACS Omega*. 2021;6(8):5670–5678. doi:10.1021/acsomega.0c06115

27. Loskutova K, Olofsson K, Hammarstroem B, Wiklund M, Svagan AJ, Grishenkov D. Measuring the Compressibility of Cellulose Nanofiber-Stabilized Microdroplets Using Acoustophoresis. *Micromachines-Basel*. 2021;12(12):1465. doi:10.3390/mi12121465

28. Svagan AJ, Benjamins JW, Al-Ansari Z, et al. Solid cellulose nanofiber based foams - Towards facile design of sustained drug delivery systems. *J Control Release*. 2016;244:74–82. doi:10.1016/j.jconrel.2016.11.009

29. Mølgaard SL, Henriksson M, Cardenas M, Svagan AJ. Cellulose-nanofiber/polygalacturonic acid coatings with high oxygen barrier and targeted release properties. *Carbohyd Polym*. 2014;114:179–182. doi:10.1016/j.carbpol.2014.08.011

30. Schindelin J, Arganda-Carreras I, Frise E, et al. Fiji: an open-source platform for biological-image analysis. *Nat Methods*. 2012;9(7):676–682. doi:10.1038/Nmeth.2019

31. Luo N, Lu YM, Jiang YB. Solubility of Paclitaxel in Mixtures of Dichloromethane and Supercritical Carbon Dioxide. *Chinese J Chem Eng*. 2011;19(4):558–564. doi:10.1016/S1004-9541(11)60021-9

32. Conover WJ. *Practical Nonparametric Statistics*. 2nd ed. Wiley; 1980.

33. Tan XY, Hamid SBA, Lai CW. Preparation of high crystallinity cellulose nanocrystals (CNCs) by ionic liquid solvolysis. *Biomass Bioenerg*. 2015;81:584–591. doi:10.1016/j.biombioe.2015.08.016

34. Pei AH, Butchosa N, Berglund LA, Zhou Q. Surface quaternized cellulose nanofibrils with high water absorbency and adsorption capacity for anionic dyes. *Soft Matter*. 2013;9(6):2047–2055. doi:10.1039/c2sm27344f

35. Bravo I, Aranda A, Hurley MD, et al. Infrared absorption spectra, radiative efficiencies, and global warming potentials of perfluorocarbons: comparison between experiment and theory. *J Geophys Res-Atmos*. 2010;115:D24317. doi:10.1029/2010jd014771

36. Sokoll R, Tiller HJ. Adsorption and reaction behavior of perfluoro-n-alkanes on Al2O3. *J Colloid Interf Sci*. 1998;205(2):489–495. doi:10.1006/jcis.1998.5638

37. Canselier JR, Delmas H, Wilhelm AM, Abismail B. Ultrasound Emulsification - An Overview. *J Disper Sci Technol*. 2002;23(1–3):333–349. doi:10.1080/01932690208984209

38. Abismail B, Canselier JP, Wilhelm AM, Delmas H, Gourdon C. Emulsification by ultrasound: drop size distribution and stability. *Ultrason Sonochem*. 1999;6(1–2):75–83. doi:10.1016/S1350-4177(98)00027-3

39. Cabrera-Trujillo MA, Filomena-Ambrosio A, Quintanilla-Carvajal MX, Sotelo-Diaz LI. Stability of low-fat oil in water emulsions obtained by ultra turrax, rotor-stator and ultrasound homogenization methods. *Int J Gastron Food S*. 2018;13:58–64. doi:10.1016/j.ijgfs.2018.06.002

40. Skale T, Stehl D, Hohl L, Kraume M, von Klitzing R, Drews A. Tuning Pickering Emulsions for Optimal Reaction and Filtration Conditions. *Chem-Ing-Tech*. 2016;88(11):1827–1832. doi:10.1002/cite.201600099

41. Wang XY, Jiang Y, Wang YW, Huang MT, Ho CT, Huang QR. Enhancing anti-inflammation activity of curcumin through O/W nanoemulsions. *Food Chem*. 2008;108(2):419–424. doi:10.1016/j.foodchem.2007.10.086

42. Taha A, Ahmed E, Ismaiel A, et al. Ultrasonic emulsification: an overview on the preparation of different emulsifiers-stabilized emulsions. *Trends Food Sci Tech*. 2020;105:363–377. doi:10.1016/j.tifs.2020.09.024

43. Kalashnikova I, Bizot H, Bertoncini P, Cathala B, Capron I. Cellulosic nanorods of various aspect ratios for oil in water Pickering emulsions. *Soft Matter*. 2013;9(3):952–959. doi:10.1039/c2sm26472b

44. Low LE, Siva SP, Ho YK, Chan ES, Tey BT. Recent advances of characterization techniques for the formation, physical properties and stability of Pickering emulsion. *Adv Colloid Interfac*. 2020;277:102117. doi:10.1016/j.cis.2020.102117

45. Wu J, Ma GH. Recent Studies of Pickering Emulsions: particles Make the Difference. *Small*. 2016;12(34):4633–4648. doi:10.1002/smll.201600877

46. Lu Y, Li J, Ge LL, Xie WY, Wu DF. Pickering emulsion stabilized with fibrous nanocelluloses: insight into fiber flexibility-emulsifying capacity relations. *Carbohyd Polym*. 2021;255:117483. doi:10.1016/j.carbpol.2020.117483

47. Lee D, Oh Y, Yoo JK, Yi JW, Um MK, Park T. Rheological study of cellulose nanofiber disintegrated by a controlled high-intensity ultrasonication for a delicate nano-fibrillation. *Cellulose*. 2020;27(16):9257–9269. doi:10.1007/s10570-020-03410-4

48. De SJ, Miller DW, Robinson DH. Effect of Particle Size of Nanospheres and Microspheres on the Cellular-Association and Cytotoxicity of Paclitaxel in 4T1 Cells. *Pharm Res-Dordr*. 2005;22(5):766–775. doi:10.1007/s11095-005-2593-8

49. Chakravarthi SS, Robinson DH. Enhanced cellular association of paclitaxel delivered in chitosan-PLGA particles. *Int J Pharmaceut*. 2011;409(1–2):111–120. doi:10.1016/j.ijpharm.2011.02.034

50. Danisman-Kalindemirtas F, Kariper IA, Hepokur C, Erdem-Kuruca S. Selective cytotoxicity of paclitaxel bonded silver nanoparticle on different cancer cells. *J Drug Deliv Sci Tec*. 2021;61doi. doi:10.1016/j.jddst.2020.102265

51. Liebmann JE, Cook JA, Lipschultz C, Teague D, Fisher J, Mitchell JB. Cytotoxic studies of paclitaxel (Taxol) in human tumor cell lines. *Brit J Cancer*. 1993;68(6):1104–1109. doi:10.1038/bjc.1993.488

52. Georgiadis MS, Russell EK, Gazdar AF, Johnson BE. Paclitaxel cytotoxicity against human lung cancer cell lines increases with prolonged exposure durations. *Clin Cancer Res*. 1997;3(3):449–454.

53. Simao CD, Reparaz JS, Wagner MR, et al. Optical and mechanical properties of nanofibrillated cellulose: toward a robust platform for next-generation green technologies. *Carbohyd Polym*. 2015;126:40–46. doi:10.1016/j.carbpol.2015.03.032

54. Jia XQ, Cai XJ, Chen Y, et al. Perfluoropentane-Encapsulated Hollow Mesoporous Prussian Blue Nanocubes for Activated Ultrasound Imaging and Photothermal Therapy of Cancer. *Acs Appl Mater Inter*. 2015;7(8):4579–4588. doi:10.1021/am507443p

55. Kandadai MA, Mohan P, Lin GY, Butterfield A, Skliar M, Magda JJ. Comparison of Surfactants Used to Prepare Aqueous Perfluoropentane Emulsions for Pharmaceutical Applications. *Langmuir*. 2010;26(7):4655–4660. doi:10.1021/la100307r

56. Nicu R, Ciolacu F, Ciolacu DE. Advanced Functional Materials Based on Nanocellulose for Pharmaceutical/Medical Applications. *Pharmaceutics*. 2021;13(8). doi:10.3390/pharmaceutics13081125

57. Colic M, Mihajlovic D, Mathew A, Naseri N, Kokol V. Cytocompatibility and immunomodulatory properties of wood based nanofibrillated cellulose. *Cellulose*. 2015;22(1):763–778. doi:10.1007/s10570-014-0524-8

58. Lopes VR, Stromme M, Ferraz N. In Vitro Biological Impact of Nanocellulose Fibers on Human Gut Bacteria and Gastrointestinal Cells. *Nanomaterials-Basel*. 2020;10(6). doi:10.3390/nano10061159

59. Malmir S, Karbalaei A, Pourmadadi M, Hamedi J, Yazdian F, Navaee M. Antibacterial properties of a bacterial cellulose CQD-TiO2 nanocomposite. *Carbohyd Polym*. 2020;234. doi:10.1016/j.carbpol.2020.115835

60. Abolghasemzade S, Pourmadadi M, Rashedi H, Yazdian F, Kianbakht S, Navaei-Nigjeh M. PVA based nanofiber containing CQDs modified with silica NPs and silk fibroin accelerates wound healing in a rat model. *J Mater Chem B*. 2021;9(3):658–676. doi:10.1039/d0tb01747g

61. Ahmadi A, Sokunbi M, Patel T, Chang MW, Ahmad Z, Singh N. Influence of Critical Parameters on Cytotoxicity Induced by Mesoporous Silica Nanoparticles. *Nanomaterials-Basel*. 2022;12(12). doi:10.3390/nano12122016

62. Hosokawa M, Hayata T, Fukuda Y, et al. Size-Selective Microcavity Array for Rapid and Efficient Detection of Circulating Tumor Cells. *Anal Chem*. 2010;82(15):6629–6635. doi:10.1021/ac101222x

63. Basti ATK, Jonoobi M, Sepahvand S, et al. Employing Cellulose Nanofiber-Based Hydrogels for Burn Dressing. *Polymers-Basel*. 2022;14(6). doi:10.3390/polym14061207

64. Ezati P, Rhim JW, Molaei R, Priyadarshi R, Han S. Cellulose nanofiber-based coating film integrated with nitrogen-functionalized carbon dots for active packaging applications of fresh fruit. *Postharvest Biol Tec*. 2022;186. doi:10.1016/j.postharvbio.2022.111845

65. Grishenkov D, Gonon A, Weitzberg E, et al. Ultrasound contrast agent loaded with nitric oxide as a theranostic microdevice. *Drug Des Dev Ther*. 2015;9:2409–2419. doi:10.2147/Dddt.S77790

66. Chumakova OV, Liopo AV, Evers BM, Esenaliev RO. Effect of 5-fluorouracil, Optison and ultrasound on MCF-7 cell viability. *Ultrasound Med Biol*. 2006;32(5):751–758. doi:10.1016/j.ultrasmedbio.2006.01.011

67. Paradossi G, Pellegretti P, Trucco A. *Ultrasound Contrast Agents: Targeting and Processing Methods for Theranostics*. 1st ed. Springer Science +Business Media; 2010.